ACS Catalysis

Research Article

pubs.acs.org/acscatalysis

Reactivity of Graphene-Supported Pt Nanocluster Arrays

Karin Gotterbarm, Florian Späth, Udo Bauer, Carina Bronnbauer, Hans-Peter Steinrück, and Christian Papp*

Lehrstuhl für Physikalische Chemie II, Universität Erlangen-Nürnberg, Egerlandstraße 3, 91058 Erlangen, Germany

Supporting Information

ABSTRACT: Nanocluster arrays on graphene (Gr) are intriguing model systems for catalysis. We studied the adsorption and oxidation of CO on Pt/Gr/Rh(111) with synchrotron-based high-resolution X-ray photoelectron spectroscopy. On the nanoclusters, CO is found to adsorb at three different sites: namely, on-top, bridge, and step. The C 1s spectra exhibit remarkable similarities to those on the stepped Pt(355) surface. Similar to the case for stepped Pt surfaces, a clear preference for the adsorption on the step sites is found, while the preference for the adsorption on the on-top site over the bridge site on the terraces is much less pronounced in comparison to that on Pt single crystals. Temperature-programmed X-ray photoelectron spectroscopy revealed an enhanced binding energy for the cluster step sites, similar to the situation on stepped Pt surfaces. The oxidation of CO on graphene-supported Pt nanoclusters follows a pseudo-first-order rate law. Applying an Arrhenius analysis, we found an activation energy of 13 ± 4 kJ/mol, which is much smaller than that on Pt(111), due to the more reactive step and kink sites on the nanoclusters.

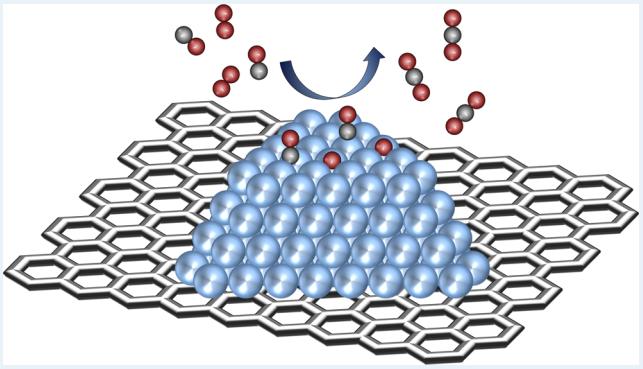

KEYWORDS: *CO oxidation, nanoclusters, platinum, graphene, HR-XPS*

INTRODUCTION

To understand catalytic processes on the atomic level, it is necessary to find suitable model systems. An appropriate model system must be simple enough to analyze it in detail yet complex enough to accurately reproduce the features of a real catalyst.[1,2] Surface science started from the most simple model systems imaginable: that is, well-oriented single-crystal surfaces such as the (111) surface of Pt. The adsorption of CO on Pt(111) was studied extensively with a variety of different methods: e.g., X-ray photoelectron spectroscopy (XPS),[3,4] infrared spectroscopy,[5] electron energy loss spectroscopy,[6] low-energy electron diffraction (LEED),[7] and density functional theory.[8] CO binds at on-top and bridge sites on Pt(111).[3−7] From a detailed thermodynamic approach, which was based on a variety of experimental data, the on-top site was found to be more stable than the bridge site by 9.1 kJ/mol (95 meV).[9] Furthermore, the oxidation kinetics of CO on Pt(111) was investigated:[10] isothermal XPS measurements at temperatures between 280 and 305 K were employed to determine the activation energy of 51 kJ/mol from an Arrhenius plot, in very good agreement with results obtained by STM.[10,11] It was found that the reaction mainly takes place at the edges of oxygen islands.[11] In order to introduce more complexity, stepped single crystals such as Pt(355) and Pt(322) were studied.[12,13] The two surfaces both consist of five-atom-wide (111) terraces but differently oriented steps. In the case of Pt(355), the steps have (111) orientation, while for Pt(322) their orientation is (100). The introduction of steps provides new adsorption sites for CO: on Pt(355), an additional CO species was detected in XPS, due to CO adsorbed in step sites.[12,13] On Pt(322), two different step adsorption sites were observed: step on-top and step bridge.[13] In addition, the adsorption behavior of CO on the (111) terraces of the stepped crystals was found to be different from that on Pt(111) due to the electronic influence of the steps. The preference for the terrace on-top site was less pronounced on Pt(322) than on Pt(111) and even less on Pt(355). These examples show that the introduction of more complexity can lead to significant changes in the adsorption behavior on the model catalysts. To move even closer to real applications and to get a satisfying model for a technical catalyst, it is necessary to introduce further complexity: e.g., by studying the reactivity of nanoparticles. However, the direct investigation of industrial catalysts is still out of the scope of model studies, as they exhibit a number of undesirable features, such as substrate-related spillover and reverse spillover effects that are difficult to avoid in oxide-supported catalyst materials.[2,14] Such effects can also be present for nanoparticles on noninnocent oxidic model supports.[15] Furthermore, the broad size distribution and varying shape of metal particles on technical catalysts

Received: February 5, 2015
Revised: March 2, 2015
Published: March 4, 2015

DOI: 10.1021/acscatal.5b00245
ACS Catal. 2015, 5, 2397−2403

necessarily complicate the identification of size-dependent effects.[16−19] Hence, regularly arranged nanoparticles with a narrow size distribution on a chemically inert substrate represent a desirable model system. It has recently been shown that such nanoparticle arrays can be produced using the template effect of graphene (Gr) Moiré structures on lattice-mismatched substrates.[20−22] Regular arrays of nanoclusters were produced by depositing a number of different metals on Gr/Ir(111).[20] For Pt nanoparticles on Gr/Ir(111), the adsorption of CO was found to induce Smoluchowski ripening.[23] Recently, we reported the fabrication of Pd nanoparticle arrays on Gr/Rh(111)[21] and used CO as a probe molecule to confirm a narrow size distribution.[24]

In this study, we present high-resolution X-ray photoelectron spectroscopy (HRXPS) results of Pt nanocluster arrays deposited on Gr/Rh(111). We investigated the adsorption of CO and the isothermal oxidation of CO on the Pt nanoclusters in detail. Further insights are gained from a comparison with earlier results on different single-crystal surfaces.[3,9,10,12,13]

EXPERIMENTAL DETAILS

The experiments were carried out at beamline U49/2-PGM1 of Helmholtz-Zentrum Berlin in a transportable UHV apparatus consisting of two chambers.[25] The analysis chamber is equipped with a hemispherical electron energy analyzer (Omicron EA 125 U7 HR) and a quadrupole mass spectrometer and is connected to the three-stage supersonic molecular beam. With this setup, pressures of up to 1×10^{-5} mbar on the sample can be achieved. The preparation chamber is equipped with an electron beam evaporator for Pt deposition and a quartz crystal microbalance (QCM) for monitoring the thickness. Resistive heating and liquid nitrogen cooling allow for sample temperatures between 100 and 1400 K. An additional filament is mounted in the back of the sample to perform linear heating ramps (0.5 K/s) during XP measurements without a disturbing influence on the measurements. Such experiments are referred to as temperature-programmed XPS (TP-XPS).[3,26] Graphene was prepared by chemical vapor deposition (CVD) of 2×10^{-8} mbar propene or ethene at 920 K. Platinum was deposited by electron beam evaporation, and the amount of deposited platinum was calibrated using the QCM. Carbon monoxide and oxygen were dosed with the molecular beam, either directly onto the sample or by backfilling the chamber (by introducing a flag in the beam path). Exposures are given in Langmuirs (L, 1.33×10^{-6} mbar s). All XP spectra were recorded in normal emission. The excitation energies were 380 eV for C 1s core level spectra and 650 eV for O 1s core level spectra, with total energy resolutions of 150 and 320 meV, respectively. All spectra were referenced to the Fermi level and corrected with a linear background. The spectra were fitted with Doniach−Sunjic functions convoluted with a Gaussian function.[27] The fitting parameters are listed in Tables S1 and S2 in the Supporting Information. The carbon and oxygen coverages were calibrated using a reference structure of CO on Rh(111) with a coverage of 0.75 monolayer (ML).[28] One ML of CO thereby corresponds to one CO molecule per Rh surface atom. An experiment showing that CO does not adsorb on or underneath Gr/Rh(111) under the chosen conditions is given in Figure S1 in the Supporting Information.

RESULTS

CO Adsorption and Desorption. Graphene was grown on Rh(111) by CVD.[29,30] As a next step, Pt was deposited using electron beam evaporation. Thereafter, the sample was exposed to CO until saturation and annealed to 540 K once before the adsorption experiment was conducted to avoid restructuring of the Pt particles during TP-XPS.[21,31] Selected C 1s spectra during the adsorption of CO on 0.7 ML of Pt on Gr/Rh(111) at 150 K are shown in Figure 1a. The thick brown spectrum,

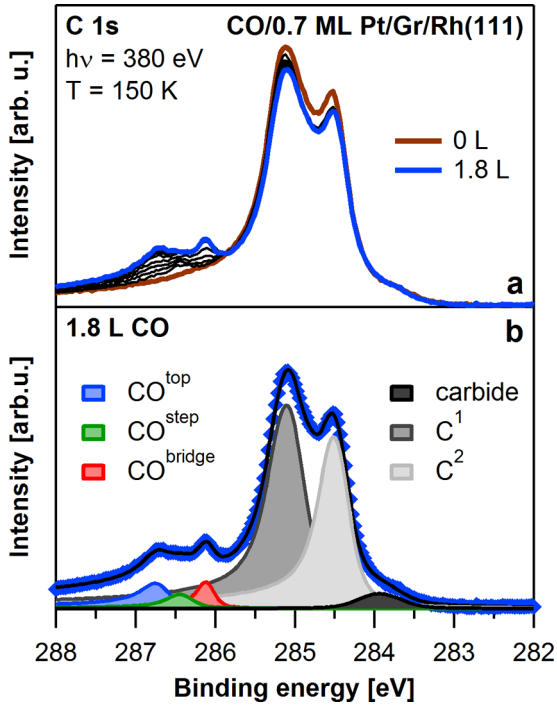

Figure 1. Adsorption of CO on 0.7 ML Pt deposited on Gr/Rh(111), at a pressure of 2.9×10^{-9} mbar: (a) Selected C 1s spectra recorded during CO adsorption at 150 K; (b) fit of the saturated spectrum after adsorption of 1.8 L of CO.

recorded before CO adsorption, shows the two characteristic signals of graphene on Rh(111) at 285.1 (C^1) and 284.5 eV (C^2).[29,30] Due to the different interaction strengths of the carbon atoms within the Moiré unit cell of graphene and the Rh(111) substrate, two C 1s signals for strongly (C^1) and weakly bonded (C^2) graphene are observed.[32,33] The small shoulder at 283.9 eV is assigned to carbidic carbon. The C 1s spectrum of graphene before Pt deposition is shown for comparison in Figure S2 in the Supporting Information.

Upon exposure to CO (thin black spectra), three additional signals evolve at 286.1, 286.5, and 286.7 eV. The comparison to single-crystal data of CO on Pt(111)[3] and stepped Pt crystals[12,13] leads to an unequivocal assignment of the three signals to different CO adsorption sites (see Figure 2). The signal at 286.1 eV corresponds to CO adsorbed at on-top sites (CO^{top}), the peak at 286.7 eV to CO at bridge sites (CO^{bridge}), and the peak at 286.5 eV to CO at step sites (CO^{step}). After saturation with CO at an exposure of 1.8 L (blue spectrum), both graphene signals are slightly damped. The fit of the saturated spectrum is shown in Figure 1b. The CO contributions in the spectrum were fitted with the same fitting parameters as used for Pt(355) and Pt(322).[12,13] The fitting parameters are given in Table S1 in the Supporting

DOI: 10.1021/acscatal.5b00245
ACS Catal. 2015, 5, 2397−2403

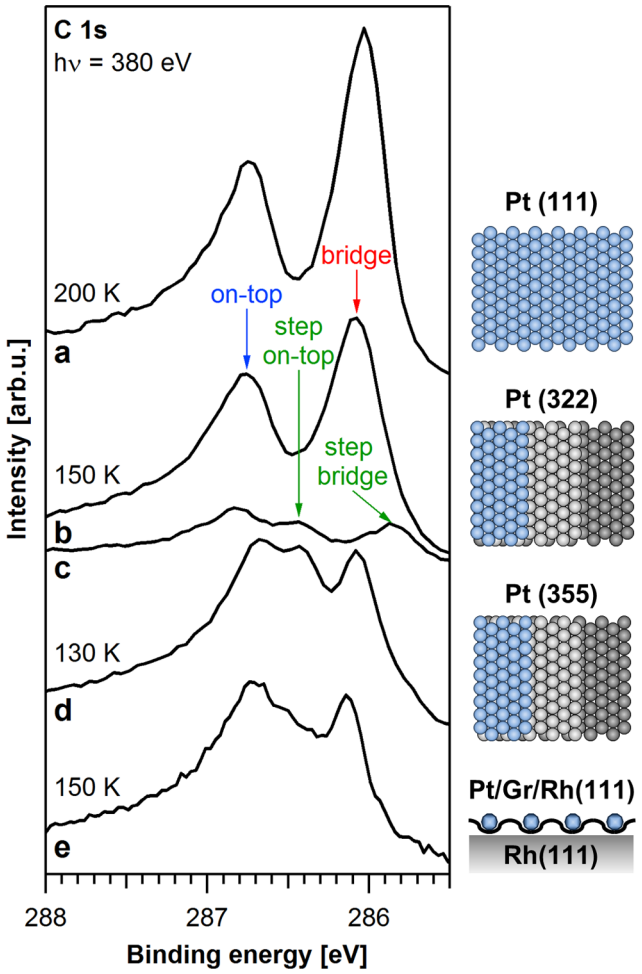

Figure 2. C 1s spectra of CO on different Pt substrates: (a) saturated CO layer on Pt(111) at 200 K;[3] (b) saturated CO layer on Pt(322) at 150 K;[13] (c) unsaturated CO layer on Pt(322) at 150 K; (d) saturated CO layer on Pt(355) at 130 K;[12,13] (e) saturated CO layer on 0.7 ML Pt nanoclusters on Gr/Rh(111) at 150 K.

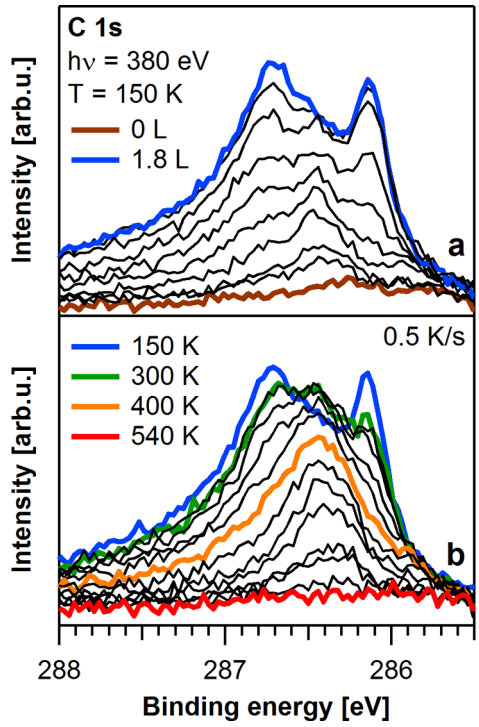

Figure 3. Selected C 1s spectra of CO on 0.7 ML Pt on Gr/Rh(111) after subtraction of the graphene and carbide signals: (a) adsorption of CO at 150 K at a pressure of 2.9×10^{-9} mbar (see also Figure 1), with thin black spectra recorded at exposures of 0.04, 0.09, 0.20, 0.31, 0.43, 0.55, 0.67, and 0.92 L, respectively; (b) TP-XPS with a linear heating rate of 0.5 K/s, with thin black spectra recorded in 20 K steps between 300 and 540 K.

Information, and additional fits are shown in Figure S3 in the Supporting Information. The graphene signals are shown in dark (C^1) and light gray (C^2), and carbidic carbon is shown in black. The three CO-induced species—on-top, step, and bridge—are displayed in blue, green, and red, respectively. As the graphene signals do not show any changes besides damping and for a more clear display of the CO signals, the fitted graphene and carbidic carbon signals were subtracted from the raw data. The resulting spectra are shown in Figure 2e (saturation spectrum) and Figure 3a. Additionally, Pt 4f spectra before and after adsorption of CO are shown in Figure S4 in the Supporting Information.

In Figure 2, a comparison of our C 1s spectra to earlier measurements of CO on different Pt substrates is depicted. Spectrum (a) represents a saturated CO layer on Pt(111) at 200 K. The two distinct peaks at 286.0 and 286.8 eV stem from CO adsorbed at bridge and on-top sites, respectively.[3] Spectrum (b) shows a saturated CO layer on the stepped Pt(322) surface at 150 K.[13] Due to the similar binding energies, the two dominating signals at 286.1 and 286.8 eV are assigned to CO adsorbed at bridge and on-top sites on the (111) terraces of the surface. A detailed comparison with Pt(111) reveals additional intensity at 285.8 and 286.4 eV. In spectrum (c), which corresponds to ~30% of the saturation coverage of CO on Pt(322), this additional intensity is resolved as two distinct peaks, due to CO adsorbed at different step sites: on-top and bridge. Spectrum (d) of the saturated CO layer on Pt(355)[12,13] at 130 K exhibits three signals at 286.1, 286.4, and 286.7 eV. These are assigned to CO adsorbed at bridge, step, and on-top sites, respectively. Interestingly, only one step site with a similar binding energy as the step on-top site on Pt(322) is observed, which is attributed to the different step geometry of the Pt(355) surface.[12,13] Spectrum (e) shows the saturation spectrum of CO adsorbed on 0.7 ML Pt deposited on Gr/Rh(111) at 150 K, after the subtraction of the graphene signals (see Figure 1). The spectrum closely resembles the one from Pt(355), with three signals at 286.1, 286.5, and 286.7 eV. In analogy to Pt(355), these signals are assigned to CO adsorbed at bridge, step, and on-top sites, respectively. The intensity of the step signal at 286.5 eV is slightly lower than that on Pt(355).

The C 1s spectra collected during CO adsorption on 0.7 ML Pt/Gr/Rh(111) after subtraction of the graphene signals (see Figure 1) are displayed in Figure 3a. CO first adsorbs at step sites (286.5 eV), while the on-top and bridge sites (286.7 and 286.1 eV) are populated only at higher exposures, with the on-top sites saturating last. The initial population of step sites is even more evident from Figure 4a, where the partial CO coverages, as obtained from fitting, are plotted as a function of the CO exposure. The CO step coverage (CO^{step}, green diamonds) increases steeply to 0.024 ML at an exposure of 0.2 L CO; for higher exposures, it slowly increases further to 0.031 ML. 0.2 L also marks the onset for the occupation of top sites.

DOI: 10.1021/acscatal.5b00245
ACS Catal. 2015, 5, 2397−2403

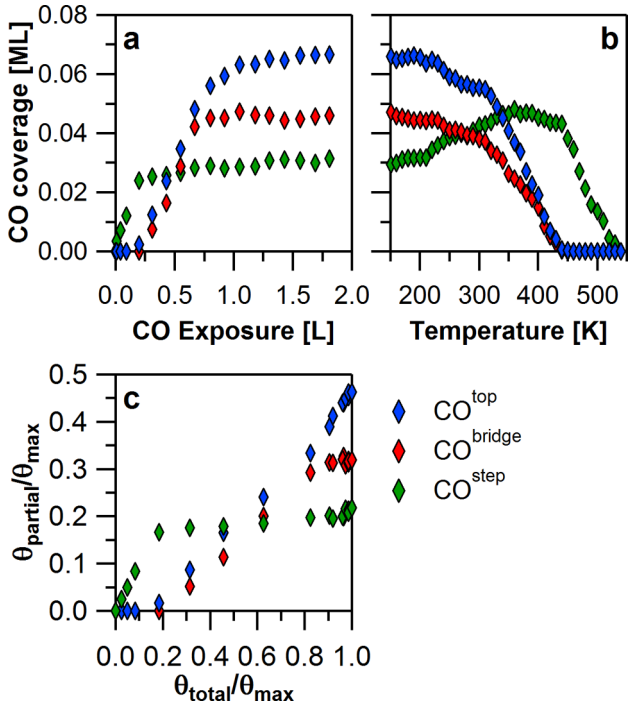

Figure 4. Partial CO coverages, as obtained from fitting of the C 1s spectra: (a) data during CO adsorption on Pt/Gr/Rh(111) at 150 K (see Figures 1 and 2a); (b) data during TP-XPS of CO on Pt/Gr/Rh(111) (see Figure 2b); (c) data of Figure 4a, normalized to maximum coverage and plotted versus normalized total coverage. This plot facilitates comparison with single-crystal data.

The CO^{top} coverage (blue) increases steeply until 0.8 L and thereafter slowly saturates at 0.066 ML at 1.6 L. The population of CO^{bridge} sites (red) begins at an exposure of 0.3 L and saturates at 0.8 L at a coverage of 0.045 ML. We repeated the adsorption of CO on several freshly prepared samples of 0.7 ML Pt/Gr/Rh(111) and found similar coverages for all CO species within the error bars of ±5%.

The data of Figure 4a are replotted in Figure 4c, where the normalized partial coverages, $\theta_{partial}/\theta_{max}$, (normalized to the maximum total coverage of 0.14 ML) are plotted versus the normalized total coverage, $\theta_{total}/\theta_{max}$. This facilitates the comparison of the CO adsorption process on Pt nanoclusters with the adsorption on different single-crystal surfaces. Similar to the situation on Pt(355) and Pt(322), a clear preference is found for adsorption at step sites.[12,13] Adsorption on bridge and on-top sites only starts after the saturation of the step sites at $\theta_{partial}/\theta_{max}$ = 0.18: that is, 18% of the total coverage. The occupation of bridge sites starts only slightly after the onset of the occupation of on-top sites. On Pt(111), a much more pronounced preference for the adsorption on the on-top sites is observed: that is, bridge occupation started only when the on-top occupation reached ~65% of its saturation value.[3] McEwen et al. determined an energy difference of 9.1 kJ/mol between the bridge and on-top adsorption sites on Pt(111).[9] The preference for on-top over bridge sites, as seen from the $\theta_{partial}/\theta_{max}$ versus $\theta_{total}/\theta_{max}$ plots, decreases in the order Pt(111), Pt(322), Pt(355), Pt nanoclusters on graphene.[12,13,25] This leads to the conclusion that the energy difference between on-top and bridge sites is reduced drastically, very likely due to electronic effects that are influenced by the terrace (facet) width and step orientation. For the saturated CO spectra, a remarkable similarity is seen for CO adsorbed on Pt nanoclusters and Pt(355) (see Figure 2d,e, respectively). This similarity indicates that the nanoclusters mostly consist of Pt(111) facets, since only one CO-induced signal in XPS was observed on Pt(100).[34−36] As only one step peak is observed, we conclude that predominantly (111) steps are occupied. On Pt(355), the CO step coverage is 17% higher than that on the Pt nanoclusters and the coverage of bridge sites is 18% lower. A comparison of the terrace/step occupancy ratio indicates a comparably low step density and larger average terrace width for the clusters relative to the Pt(355) surface.

After CO was adsorbed until saturation, the sample was heated with a linear rate of 0.5 K/s, and XP spectra were measured every 10 K. The original data of this TP-XPS experiment as well as example fits are shown in Figures S5 and S6 in the Supporting Information. Selected spectra after subtraction of the graphene-related signals are shown in Figure 3b, and the corresponding quantitative analysis is shown in Figure 4b. The blue spectrum recorded at 150 K corresponds to the last spectrum of the adsorption experiment shown in Figures 1 and 3a. When the temperature is raised to 300 K (green spectrum), the CO^{step} signal at 286.5 eV increases, while the CO^{top} and CO^{bridge} signals at 286.7 and 286.1 eV slowly decrease. At 310 K, the CO^{top} (blue diamonds in Figure 4b) and CO^{bridge} (red) coverages have slowly decreased by 17% and 21%, respectively, while the CO^{step} coverage (green) has increased by 46%. Above 310 K, the decrease of CO^{top} and CO^{bridge} accelerates, at 400 K (orange spectrum in Figure 3b) the two signals are only seen as shoulders, and at 450 K both species have completely desorbed from the nanoclusters. Above 310 K the CO^{step} coverage further increases to 0.047 ML at 340 K: that is, by a total of 58% in comparison to 150 K. This behavior indicates a reorganization of the adsorbed CO toward the energetically favorable step sites that was not possible at 150 K due to limited mobility on the partially covered surface at the lower temperature. A similar increase of the step coverage upon heating by 70% was also observed on Pt(322).[13] Between 340 and 450 K, the CO^{step} coverage then is nearly constant (within 8%) and thereafter decreases quickly to finally vanish. At 540 K (red spectrum), all CO is desorbed from the surface. It is interesting to note that the temperatures, at which CO desorption from cluster terraces (450 K) and step sites (540 K) is completed are identical to within ±10 K to the corresponding values on Pt(355) under similar conditions.[12] This similarity indicates comparable adsorption energies at the respective sites for both systems.

Isothermal CO Oxidation. In addition to the adsorption and desorption behavior of CO, we also investigated the oxidation of CO on Pt nanoclusters deposited on Gr/Rh(111) under isothermal conditions. Figure 5a shows selected O 1s spectra during the oxidation of CO at 250 K. The green spectrum was recorded after the surface was saturated with oxygen (6 L). The spectrum exhibits one asymmetric signal at 529.8 eV due to atomic oxygen, which is known to form on Pt(111) upon O_2 exposure at 150 K.[37,38] After saturation with oxygen, the surface was exposed to the supersonic molecular beam of CO with a pressure of 2.6×10^{-7} mbar on the sample. With increasing CO exposure (black spectra in Figure 5a), the atomic oxygen related signal decays and two CO induced signals evolve at 531.2 and 532.7 eV. The last spectrum (blue) was recorded after 360 s. At this exposure, the signal due to atomic oxygen has vanished and the two CO induced signals are saturated. Note that this spectrum resembles that obtained after exposure of oxygen-free Pt nanoclusters deposited on Gr/

DOI: 10.1021/acscatal.5b00245
ACS Catal. 2015, 5, 2397−2403

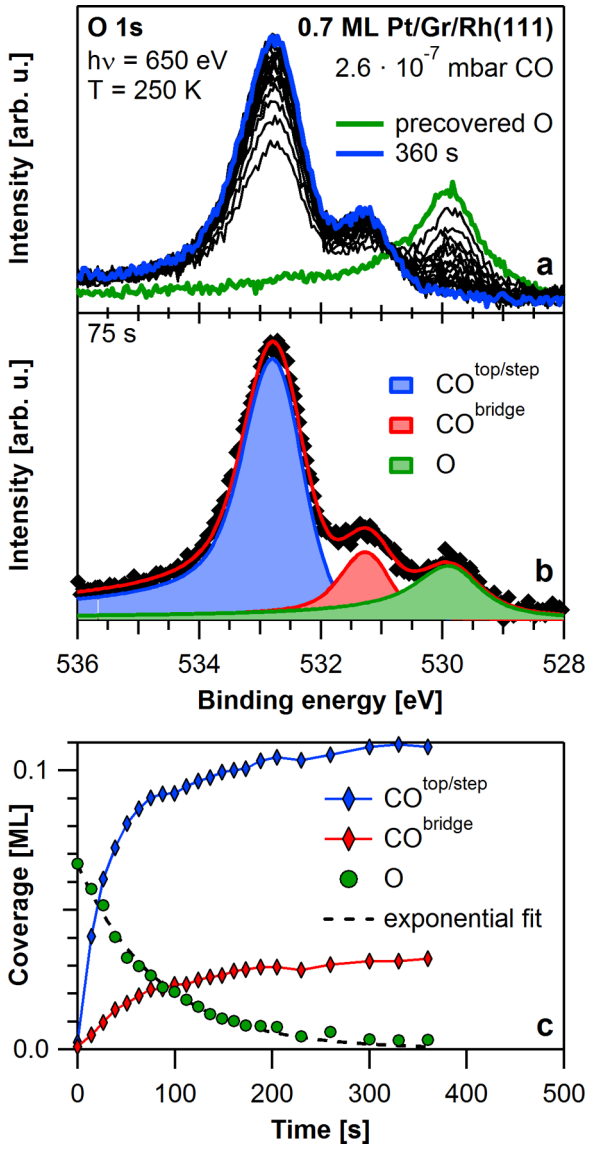

Figure 5. Isothermal oxidation of CO on 0.7 ML Pt/Gr/Rh(111) at 250 K: (a) selected O 1s spectra during CO adsorption on oxygen precovered nanoclusters, at a constant CO pressure of 2.6×10^{-7} mbar; (b) fit of an intermediate spectrum measured at 75 s CO exposure; (c) fitting results of the experiment shown in (a), with the oxygen coverage fitted with an exponential function and red and blue lines as a guide to the eye.

Rh(111) to CO. The fit of the intermediate spectrum recorded after 75 s is shown in Figure 5b. The fitting parameters are given in Table S2 in the Supporting Information. The spectrum was fitted with three contributions: atomic oxygen at 529.8 eV (green) and two CO signals at 531.2 and 532.7 eV (red and blue). Interestingly, only two CO-derived peaks are observed, which have binding energies similar to those found for CO on Pt(111), where the signals are attributed to CO adsorbed at bridge and on-top sites, respectively.[10] The difference to Pt(111) is a larger full width at half-maximum (fwhm) of the signal at 532.7 eV by 70 meV, due to the fact that this signal is composed not only of CO at on-top sites but also of CO at step sites. Due to the overlap of the two signals, a distinction between CO at on-top and step sites is ambiguous in the O 1s spectra. Since the focus of our kinetic analysis is on the coverage of atomic oxygen, we thus used only one contribution to account for CO adsorbed at on-top and step sites. The quantitative analysis resulting from the fitting procedure of all spectra is shown in Figure 5c. The CO on-top plus step coverage is displayed as blue diamonds and the CO bridge coverage as red diamonds, with the thin blue and red lines as guides to the eye. Upon CO exposure, we observe a fast increase of the $CO^{top/step}$ coverage, which slows down around 70 s and saturates at 0.11 ML above 300 s. For CO^{bridge} an overall similar behavior is found: after a less steep initial increase until around 70 s, it slowly increases further to finally saturate at 0.03 ML after 250 s. The decay of atomic oxygen (green circles) can very well be described by an exponential decay (dashed black line) toward a minimum coverage of 0.003 ML, reached after 300 s. This exponential decrease of the oxygen coverage is a strong indicator for pseudo-first-order reaction kinetics. Since CO is provided in excess from the molecular beam, the local coverage of CO in the vicinity of oxygen is assumed as constant once the surface is saturated with CO (which should be achieved after 5 s at the applied pressure). In this case, the reaction rate only depends on the coverage of oxygen on the surface and not on the CO pressure in the gas phase. This is confirmed by experiments at higher pressures yielding similar pseudo first-order reaction kinetics (data not shown).

To gain more insight into the reaction kinetics, we performed isothermal CO oxidation experiments also at different temperatures (but otherwise identical conditions) on the Pt nanoclusters and compared the results to those obtained for Pt(111). In Figure 6a, the decrease of the oxygen coverage during CO exposure at 290 K (red circles) is shown along with a similar experiment on Pt(111) (gray squares, reproduced from ref 10) at the same temperature; in both cases the oxygen coverages have been normalized to the value at $t = 0$ s. The Pt nanocluster data (red circles) can be described well by an exponential function (dashed red line), again confirming the assumption of pseudo-first-order kinetics. In contrast, a function assuming a 0.63 order rate law (dotted line) had to be used to describe the Pt(111) data. This is due to the fact that on Pt(111) the reaction of CO with atomic oxygen mainly takes place at the edges of two-dimensional oxygen islands. Therefore, the reaction order is closer to 0.5 than to 1 (see refs 10 and 11 for more details). Due to the smaller terrace size on the Pt nanoclusters, only small or no oxygen islands form, and thus reaction at island borders does not play a role. Therefore, the reaction on the clusters is sufficiently well described by the simpler pseudo-first-order rate law. Note that also on Pt(111) much faster reaction rates were observed for disordered oxygen at the beginning of the oxidation reaction.[10] This faster reaction channel could be related to the pseudo-first-order kinetics that we observe on the Pt clusters.

The complete series of isothermal CO oxidation experiments is shown in a logarithmic plot in Figure 6b. All experiments were conducted with a CO pressure of 2.6×10^{-7} mbar on the sample. The oxygen coverages at $t = 0$ s vary by only ±3% and are normalized to 100% for convenience. From this graph, it is evident that the description with a pseudo-first-order rate law is applicable. The data at 290 K (red circles, see also Figure 6a), 270 K (orange), and 250 K (green; see also Figure 5) are described well by straight lines in the logarithmic plot, down to 10% of the initial coverage. For longer reaction times, minor deviations from the fits are observed. Only at 230 K (blue), the fitting with a linear function is satisfactory only to ~40% of the initial coverage (that is, in the first 100 s); at longer reaction

DOI: 10.1021/acscatal.5b00245
ACS Catal. 2015, 5, 2397−2403

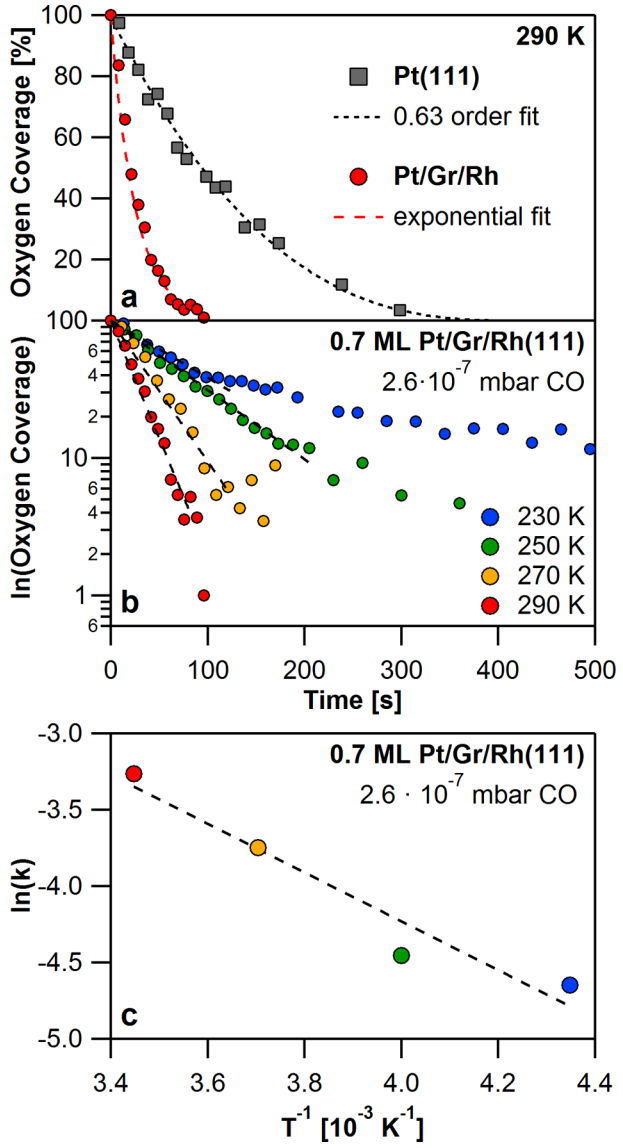

Figure 6. (a) Comparison of the CO oxidation kinetics at 290 K, on Pt(111) (gray squares, data from ref 10) and 0.7 ML Pt/Gr/Rh(111). The Pt(111) data are fitted with a 0.63-order rate law (dotted line, see ref 10), and the nanocluster data are fitted with a pseudo-first-order rate law (dashed line). (b) Logarithmic plot of a series of isothermal oxidation experiments on 0.7 ML Pt/Gr/Rh(111) at varying temperatures, fitted with pseudo-first-order rate laws (dashed lines). (c) Arrhenius analysis of the reaction constants derived from the fits in (b).

times, oxidation proceeds at a lower rate. One possible explanation is that at 230 K the mobility of the adsorbates on the nanocluster facets is reduced and the optimum reaction geometry cannot be reached fast enough.[39,40] As a consequence, the reaction would proceed more slowly after neighboring reactants are consumed. Note that 230 K marks the onset of an increased step population upon heating a saturated (pure) CO layer in Figure 4b.

The rate constants, *k*, obtained from the linear fits in Figure 6b are displayed as colored circles in the Arrhenius plot in Figure 6c. From the negative slope, the activation energy of the CO oxidation process is determined to be 13.3 ± 4.0 kJ/mol. The large uncertainty results from error bars of the determination of the rate constants in Figure 6b. In addition to the experiment at 2.6 × 10^{-7} mbar, we also studied the reaction at a higher pressure of 2.1 × 10^{-6} mbar; the resulting activation energy of 11.4 kJ/mol falls well within the denoted error bars. The activation energy observed for the clusters is significantly smaller than the values of 51 ± 4 and 47 ± 4 kJ/mol determined for the same reaction on Pt(111) by XPS and STM, respectively.[10,11] This is attributed to the higher reactivity of step and kink sites on the nanoclusters.[41] In contrast, Meusel et al. studied CO oxidation on alumina-supported Pd nanoparticles and found the activation energies to be consistent with single-crystal data.[42] This discrepancy can possibly be explained by the different adsorption properties of the two catalytic metals. On stepped Pd surfaces, no significant preference for CO adsorption in step sites was observed,[43,44] and therefore the steps do not play as a significant role on Pd clusters as on Pt clusters.

CONCLUSION

We investigated the adsorption and oxidation of CO on graphene-supported Pt nanoclusters. Upon CO adsorption at 150 K, we observe three species in the C 1s region that are assigned to different adsorption sites—on-top, bridge, and step—in comparison to single-crystal data. We find a clear preference for the adsorption at step sites. However, the preference for on-top over bridge adsorption sites on the terraces of the nanoparticles is much less pronounced than that on Pt single crystals. By temperature-programmed experiments, we observe that the step site is the most stable adsorption site for CO. The desorption temperatures are in good agreement with those on Pt single crystals. We also investigated the isothermal oxidation of CO on the Pt nanoclusters. We find pseudo-first-order kinetics for the decay of the oxygen signal. The pseudo-first-order rate law indicates that oxygen island edges do not play a role due to the small facets of the particles. We were able to determine an activation energy of 13 ± 4 kJ/mol by Arrhenius analysis.

ASSOCIATED CONTENT

Supporting Information

The following file is available free of charge on the ACS Publications website at DOI: 10.1021/acscatal.5b00245.

Tables of the fitting parameters, example fits, the original data of the TPXPS experiment in Figure 3b, and additional Pt 4f and C 1s core level spectra (PDF)

AUTHOR INFORMATION

Corresponding Author

*E-mail for C.P.: christian.papp@fau.de.

Notes

The authors declare no competing financial interest.

ACKNOWLEDGMENTS

We thank the HZB for the allocation of synchrotron radiation beamtime. This work was supported by SFB 953 "Synthetic Carbon Allotropes" and the Cluster of Excellence "Engineering of Advanced Materials". K.G. thanks the "Fonds der chemischen Industrie" for her Ph.D. grant.

REFERENCES

(1) Freund, H.-J.; Bäumer, M.; Libuda, J.; Risse, T.; Rupprechter, G.; Shaikhutdinov, S. *J. Catal.* **2003**, *216*, 223−235.

DOI: 10.1021/acscatal.5b00245
ACS Catal. 2015, 5, 2397−2403

(2) Schauermann, S.; Nilius, N.; Shaikhutdinov, S.; Freund, H.-J. *Acc. Chem. Res.* **2012**, *46*, 1673−1681.
(3) Kinne, M.; Fuhrmann, T.; Whelan, C. M.; Zhu, J. F.; Pantförder, J.; Probst, M.; Held, G.; Denecke, R.; Steinrück, H.-P. *J. Chem. Phys.* **2002**, *117*, 10852−10859.
(4) Norton, P. R.; Goodale, J. W.; Selkirk, E. B. *Surf. Sci.* **1979**, *83*, 189−227.
(5) Schweizer, E.; Persson, B. N. J.; Tüshaus, M.; Hoge, D.; Bradshaw, A. M. *Surf. Sci.* **1989**, *213*, 49−89.
(6) Froitzheim, H.; Hopster, H.; Ibach, H.; Lehwald, S. *Appl. Phys.* **1977**, *13*, 147−151.
(7) Zasada, I.; Van Hove, M. A. *Surf. Rev. Lett.* **2000**, *07*, 15.
(8) Orita, H.; Itoh, N.; Inada, Y. *Chem. Phys. Lett.* **2004**, *384*, 271−276.
(9) McEwen, J. S.; Payne, S. H.; Kreuzer, H. J.; Kinne, M.; Denecke, R.; Steinrück, H.-P. *Surf. Sci.* **2003**, *545*, 47−69.
(10) Kinne, M.; Fuhrmann, T.; Zhu, J. F.; Whelan, C. M.; Denecke, R.; Steinrück, H.-P. *J. Chem. Phys.* **2004**, *120*, 7113.
(11) Völkening, S.; Wintterlin, J. *J. Chem. Phys.* **2001**, *114*, 6382−6395.
(12) Tränkenschuh, B.; Fritsche, N.; Fuhrmann, T.; Papp, C.; Zhu, J. F.; Denecke, R.; Steinrück, H.-P. *J. Chem. Phys.* **2006**, *124*, 074712.
(13) Tränkenschuh, B.; Papp, C.; Fuhrmann, T.; Denecke, R.; Steinrück, H.-P. *Surf. Sci.* **2007**, *601*, 1108−1117.
(14) Freund, H.-J. *Surf. Sci.* **2002**, *500*, 271−299.
(15) Vayssilov, G. N.; Lykhach, Y.; Migani, A.; Staudt, T.; Petrova, G. P.; Tsud, N.; Skála, T.; Bruix, A.; Illas, F.; Prince, K. C.; Matolín, V.; Neyman, K. M.; Libuda, J. *Nat. Mater.* **2011**, *10*, 310−315.
(16) Heiz, U.; Sanchez, A.; Abbet, S.; Schneider, W. D. *J. Am. Chem. Soc.* **1999**, *121*, 3214−3217.
(17) Maillard, F.; Savinova, E. R.; Stimming, U. *J. Electroanal. Chem.* **2007**, *599*, 221−232.
(18) Mavrikakis, M.; Bäumer, M.; Freund, H.-J.; Norskov, J. K. *Catal. Lett.* **2002**, *81*, 153−156.
(19) Frank, M.; Andersson, S.; Libuda, J.; Stempel, S.; Sandell, A.; Brena, B.; Giertz, A.; Brühwiler, P. A.; Bäumer, M.; Mårtensson, N.; Freund, H.-J. *Chem. Phys. Lett.* **1997**, *279*, 92−99.
(20) N'Diaye, A. T.; Gerber, T.; Busse, C.; Myslivecek, J.; Coraux, J.; Michely, T. *New J. Phys.* **2009**, *11*, 103045.
(21) Gotterbarm, K.; Steiner, C.; Bronnbauer, C.; Bauer, U.; Steinrück, H.-P.; Maier, S.; Papp, C. *J. Phys. Chem. C* **2014**, *118*, 15934−15939.
(22) Pan, Y.; Gao, M.; Huang, L.; Liu, F.; Gao, H.-J. *Appl. Phys. Lett.* **2009**, *95*, 093106.
(23) Gerber, T.; Knudsen, J.; Feibelman, P. J.; Grånäs, E.; Stratmann, P.; Schulte, K.; Andersen, J. N.; Michely, T. *ACS Nano* **2013**, *7*, 2020−2031.
(24) Gotterbarm, K.; Bronnbauer, C.; Bauer, U.; Papp, C.; Steinrück, H.-P. *J. Phys. Chem. C* **2014**, *118*, 25097−25103.
(25) Denecke, R.; Kinne, M.; Whelan, C. M.; Steinrück, H.-P. *Surf. Rev. Lett.* **2002**, *9*, 797−801.
(26) Baraldi, A.; Comelli, G.; Lizzit, S.; Cocco, D.; Paolucci, G.; Rosei, R. *Surf. Sci.* **1996**, *367*, L67−L72.
(27) Doniach, S.; Šunjić, M. *J. Phys. C: Solid State Phys.* **1970**, *3*, 285−291.
(28) Thiel, P. A.; Williams, E. D.; Yates, J. T., Jr; Weinberg, W. H. *Surf. Sci.* **1979**, *84*, 54−64.
(29) Gotterbarm, K.; Zhao, W.; Höfert, O.; Gleichweit, C.; Papp, C.; Steinrück, H.-P. *Phys. Chem. Chem. Phys.* **2013**, *15*, 19625−19631.
(30) Preobrajenski, A. B.; Ng, M. L.; Vinogradov, A. S.; Martensson, N. *Phys. Rev. B: Condens. Matter Mater. Phys.* **2008**, *78*, 073401.
(31) Heemeier, M.; Stempel, S.; Shaikhutdinov, S. K.; Libuda, J.; Bäumer, M.; Oldman, R. J.; Jackson, S. D.; Freund, H.-J. *Surf. Sci.* **2003**, *523*, 103−110.
(32) Iannuzzi, M.; Hutter, J. *Surf. Sci.* **2011**, *605*, 1360−1368.
(33) Voloshina, E. N.; Dedkov, Y. S.; Torbrügge, S.; Thissen, A.; Fonin, M. *Appl. Phys. Lett.* **2012**, *100*, 241606.
(34) Brodén, G.; Pirug, G.; Bonzel, H. P. *Surf. Sci.* **1978**, *72*, 45−52.
(35) Rienks, E. D. L.; Bakker, J. W.; Baraldi, A.; Carabineiro, S. A. C.; Lizzit, S.; Weststrate, C. J.; Nieuwenhuys, B. E. *Surf. Sci.* **2003**, *532*−*535*, 120−125.
(36) Rienks, E. D. L.; Bakker, J. W.; Baraldi, A.; Carabineiro, S. A. C.; Lizzit, S.; Weststrate, C. J.; Nieuwenhuys, B. E. *J. Chem. Phys.* **2003**, *119*, 6245−6252.
(37) Gland, J. L.; Sexton, B. A.; Fisher, G. B. *Surf. Sci.* **1980**, *95*, 587−602.
(38) Steininger, H.; Lehwald, S.; Ibach, H. *Surf. Sci.* **1982**, *123*, 1−17.
(39) Hoffmann, J.; Schauermann, S.; Hartmann, J.; Zhdanov, V. P.; Kasemo, B.; Libuda, J.; Freund, H.-J. *Chem. Phys. Lett.* **2002**, *354*, 403−408.
(40) Brandt, B.; Schalow, T.; Laurin, M.; Schauermann, S.; Libuda, J.; Freund, H.-J. *J. Phys. Chem. C* **2006**, *111*, 938−949.
(41) Vajda, S.; Pellin, M. J.; Greeley, J. P.; Marshall, C. L.; Curtiss, L. A.; Ballentine, G. A.; Elam, J. W.; Catillon-Mucherie, S.; Redfern, P. C.; Mehmood, F.; Zapol, P. *Nat. Mater.* **2009**, *8*, 213−1122.
(42) Meusel, I.; Hoffmann, J.; Hartmann, J.; Heemeier, M.; Bäumer, M.; Libuda, J.; Freund, H.-J. *Catal. Lett.* **2001**, *71*, 5−13.
(43) Conrad, H.; Ertl, G.; Koch, J.; Latta, E. E. *Surf. Sci.* **1974**, *43*, 462−480.
(44) Zhang, J.; Zhang, X.; Wang, Z.; Diao, Z. *Appl. Surf. Sci.* **2008**, *254*, 6327−6331.

DOI: 10.1021/acscatal.5b00245
ACS Catal. 2015, 5, 2397−2403